

## Thermo-mechanical fatigue crack propagation experiments in IN718

Lars Jacobsson<sup>1</sup>, Christer Persson<sup>1</sup>, Solveig Melin<sup>2</sup>

<sup>1</sup>Division of Materials Engineering, Lund University

<sup>2</sup>Division of Mechanics, Lund University

Box 118, 221 00 Lund, Sweden

**Keywords:** Thermo-mechanical fatigue, crack propagation, potential drop, Inconel 718

**Abstract.** An experimental test facility to perform thermo-mechanical fatigue crack growth experiments was developed. The thermal cycles were generated using hot and cold air flows distributed by a nozzle onto the test specimen. The crack length and the crack closure level were determined using the potential drop technique. Thermo-mechanical fatigue crack propagation experiments, strain controlled with high strain ranges, were performed in-phase and out-of-phase with various  $R$ -values on samples of Inconel 718. It was found that the temperature at which the maximum mechanical load is applied is decisive for the crack propagation rate.

### Introduction

In many applications components are subjected to alternating mechanical loads as well as to variations in temperature. One typical example is components in gas turbines, where changes in effect out-take, or start-up and shut-down sequences, induce variations in mechanical as well in thermal loads. In such situations cracks might be nucleated and propagate to failure of the component under conditions termed as thermo-mechanical fatigue (TMF).

There are, relatively speaking, few studies published on crack propagation under TMF loading conditions, as compared to studies concerning iso-thermal situations where crack propagation is studied at constant temperatures. For references and discussions cf. e.g. [1] – [6]. In this study, an experimental technique to enable in-phase as well as out-of-phase thermo-mechanical fatigue crack propagation experiments is presented. Using the present technique, thermo-mechanical  $da/dN$ -curves obtained under different TMF cycle conditions are compared to find characteristics affecting the crack propagation rate.

### Experimental procedure

The test specimens were cylindrical, smoothed and with a diameter of 6.3 mm. The specimens were prepared with a notch through spark machining to an approximate size of width×depth×height=150×150×75  $\mu\text{m}$ .

The material in this study was Inconel 718, with material properties found in Table 1. Here,  $\sigma_{ys}$  denotes the yield stress,  $E$  the modulus of elasticity, and  $\bar{\alpha}$  the mean value of the coefficient of thermal expansion in the interval from room temperature to maximum experimental temperature. The specimen surface temperature was measured by a thermocouple close to the crack plane, at the position denoted  $T$  in Figure 1, showing a schematic of the experimental equipment to obtain the thermo-mechanical load cycles.

The mechanical loading was provided by a MTS servo hydraulic load frame. The mechanical cycles were displacement controlled, and the specimen elongation measured by an extensometer with measuring points 12 mm apart. The thermal cycling was hot and cold air convection based. Two Leister fans (a in Figure 1) produced a continuous room temperature air flow of 1100 l/min. One of the fans was connected to a Leister air heater (b in Figure 1), with an outlet temperature of 900°C. The two air flows were alternately directed at the test specimen, enabling heating and

cooling during chosen periods of time. The air flow was distributed over the test specimen surface using a nozzle (e in Figure 1) to minimize temperature gradients, both circumferential and along the test specimen. The air flows were channeled into the nozzle through 62 mm pipes that were moved sideways by a pneumatic piston (c in Figure 1), changing the airflow between hot and cold. The speed of the piston was adjustable to provide suitable cycle characteristics.

The crack length was measured using the PD technique, cf. [7], [8], with a direct current of 7A passing through the specimen through thin wires of Inconel 718, welded close to the notch. A reference signal was obtained by placing two wires at the opposite side of the specimen with respect to the crack, to measure eventual divergences in the PD signal due to i.e. room temperature changes. The crack length was determined from the PD measurements through

$$a = a_{start} + f_{PD} (PD_{measured} - PD_0) \quad (1)$$

where  $a$  is the current crack length,  $a_{start}$  is the crack length when the TMF cycling starts,  $f_{PD}$  is an experimentally obtained calibration function,  $PD_{measured}$  the ratio between the PD signal taken over the crack and the reference PD signal, and  $PD_0$  the corresponding ratio from when the crack length was  $a_{start}$ .

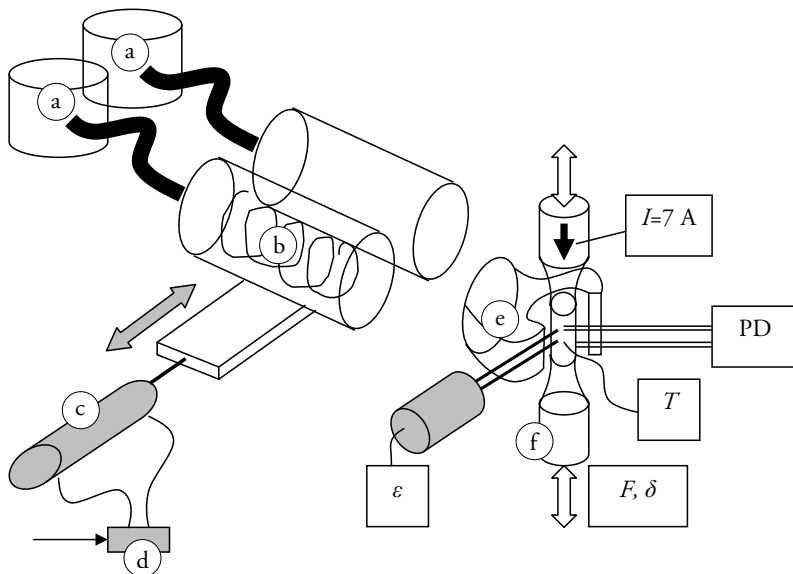


Figure 1. The TMF test facility. The recorded parameters  $F$  (force),  $\delta$  (displacement), and  $\epsilon$  (strain) are fed in to the Instron 8500+ steering tower that controls the load frame.  $T$  (temperature) and PD-signal are monitored by a computer. A current of 7 A is passed through the test specimen to generate the electrical potential drop along the specimen. a) Two Leister fans producing an air flow of 1100 l/min, b) Leister air heater with output air temperature 900°C, c) pneumatic piston changing the air flow pips through the nozzle between hot and cold, d) magnetic valve to control the pneumatic piston, e) nozzle distributing the air flow over the test specimen to minimize thermal gradients.

Table 1. Material properties of Inconel 718.

Temperature (°C)	$\sigma_{ys}$ (MPa)	$E$ (GPa)	Electrical resistivity ( $\mu\Omega/\text{cm}$ )	$\bar{\alpha}$ ( $\mu\text{m}/\text{m}^\circ\text{C}$ )
Room temperature	1175	200	121	12.6
200	1080	191	125	13.5
550	995	167	131	14.5

Table 2. Specification of experiments E1–E7.

Experiment	$T_{min}-T_{max}$	$\Delta\varepsilon$	$R_\varepsilon$	$U_\varepsilon$	TMF cycle
E1	200–550°C	0.38%	0.5	1.0	In phase
E2	200–550°C	0.75%	0	0.83	In phase
E3	200–550°C	0.92%	-1	0.64	In phase
E4	200–550°C	0.75%	0	0.66	Out of phase
E5	200–550°C	0.85%	-1	0.57	Out of phase
E6	200–550°C	1.01%	-1	0.60	Out of phase
E7	200–550°C	1%	-2.2	0.50	Out of phase

A steering program, using the National Instruments LabView, was developed to control the cycle parameters and the heating device, and to store applied load, displacement, strain, temperature, and PD signals with filtering of the signals if necessary, and a galvanic bridge preventing creep currents that otherwise could affect the recorded temperature level.

The crack was initiated at a load level of 50 % of the yield stress at room temperature until a crack of length of about 0.3–0.5 mm was obtained. When the thermal cycles were stabilized, compensation for thermal expansion was made through measuring the thermal strains during cycling of the temperature at zero mechanical load. These strains were accounted for by adding them into the steering program to compensate the thermal strains when cycling thermo-mechanically. The thermal cycles lasted two minutes each, with the temperature raised from 200°C up to 550°C and then lowered back to 200°C. The cracks were propagated under TMF load cycles to a final length of about 2–3 mm, where after the cycling was stopped and the test specimens

broken under tensile loading. The radial thermal gradient was adjusted through the cycles to be kept below 10°C as determined through finite element calculations.

After breaking a specimen, two well defined crack profiles were observed on the fracture surface from changes in color. One showed where the TMF cycling had started, and one the crack profile at final fracture. The shapes of the cracks were found to remain self-similar throughout the experiments.

Seven experiments, E1–E7, were performed. The load cycles were TMF crack propagation in-phase (IP) and out-of-phase (OP) cycles. Parameters as cycle type, strain range  $\Delta\varepsilon = \varepsilon_{max} - \varepsilon_{min}$ , and strain ratio  $R_c = \varepsilon_{min} / \varepsilon_{max}$  for each experiment are shown in

Table 2.

## Results and Discussion

### Crack closure

The crack closure level is found to have a significant influence on the crack propagation rate. In Figure 2, showing the upper right part of the load versus the thermally compensated PD-signal, a well distinguished change in slope identifies the crack closure level during unloading, marked in the figure by a horizontal line. The strain level at crack closure was found to remained constant throughout the experiments as found through investigating the thermal response in PD signal for different crack lengths. Therefore, the crack closure level was determined at unloading during the cycles at the end of the experiments.

The crack closure can be quantified by the crack closure level,  $U_\varepsilon$ , included in Table 2, defined by

$$U_\varepsilon = \frac{\Delta\varepsilon_{eff}}{\Delta\varepsilon} = \frac{\varepsilon_{max} - \varepsilon_{cl}}{\varepsilon_{max} - \varepsilon_{min}} \quad (2)$$

where  $\Delta\varepsilon_{eff}$  is the effective strain range compensated for crack closure,  $\Delta\varepsilon$  the strain range,  $\varepsilon_{max}$  the maximum and  $\varepsilon_{min}$  the minimum strain, and  $\varepsilon_{cl}$  the strain at which the crack closes.

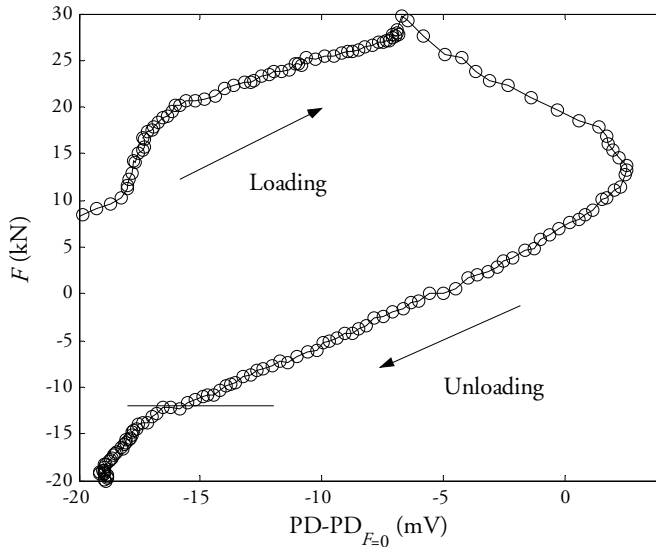


Figure 2. Applied load versus the PD signal minus the PD signal measured at zero mechanical load to compensate for thermal effects. The line marks the crack closure level.

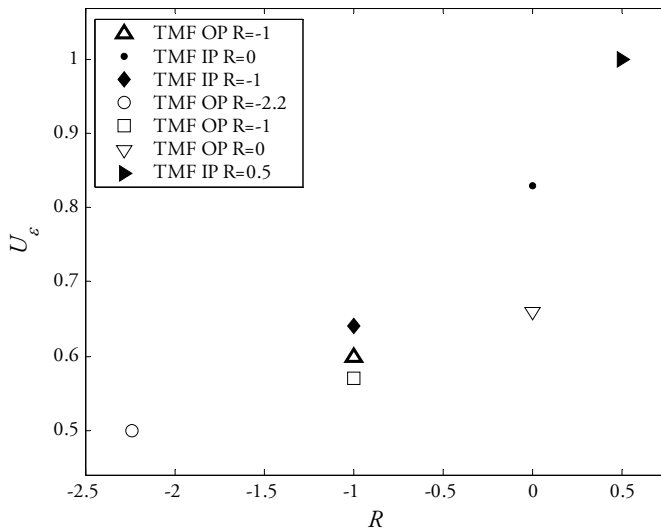


Figure 3. Crack closure level  $U_{\epsilon}$  versus strain ratio  $R_{\epsilon}$ .

Different parameters affect the closure level as discussed in e.g. [9] – [12]. An increase in strain ratio  $R_{\epsilon}$  increases the amount of plasticity during the load cycle, and the crack closure level will drop. It was also observed that TMF in-phase cycles produced lower crack closure levels than TMF out-of-phase cycles, depending on the lowered strength of the material at 550°C, where maximum load is applied at in-phase cycles. In Figure 6 the crack closure level  $U_{\epsilon}$  is seen versus strain ratio  $R_{\epsilon}$  for all experiments.

**Crack propagation rate**

In Figure 4 the crack propagation rates for experiments E1–E7 as functions of  $\Delta K$  with

$$\Delta K = \Delta\sigma\sqrt{\pi a}f(a/r, a/b) \tag{3}$$

the stress intensity factor range,  $a$  the crack length, and  $f$  a function compensating for the geometry [13].

Correlating the crack propagation rate to the effective  $J$ -integral,  $\Delta J_{eff}$ , compensated for crack closure, gives the result seen in Figure 5, where

$$\Delta J_{eff} = 2\pi a(1-\nu^2)f\Delta U_{c,eff}$$

with  $\Delta U_{c,eff}$  the strain energy density compensated for crack closure

$$\Delta U_c = \int_{\sigma_{min}}^{\sigma_{max}} (\sigma - \sigma_c) d\varepsilon$$

with  $\sigma_c$  denoting the crack closure stress.

As seen, the curves are collected properly as compared to the uncompensated curves. The TMF in-phase curves group together, as do the TMF out-of-phase curves. The scatter might be due to the relative uncertainty in determining the crack closure level.

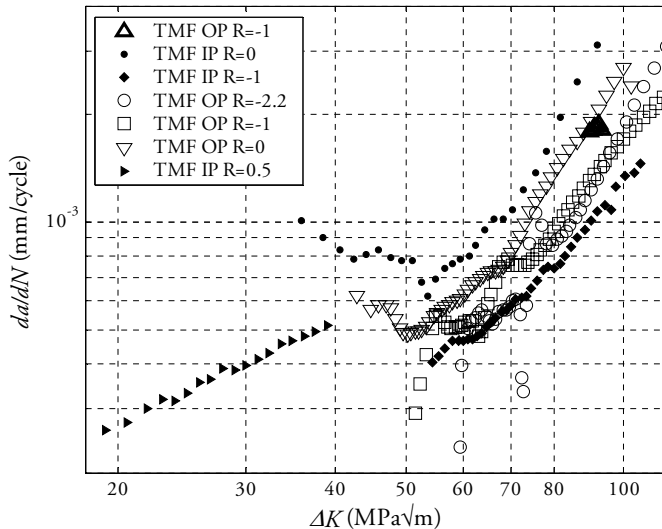


Figure 4. Crack propagation rate  $da/dN$  versus stress intensity factor range  $\Delta K$  for the experiments in Table 2.

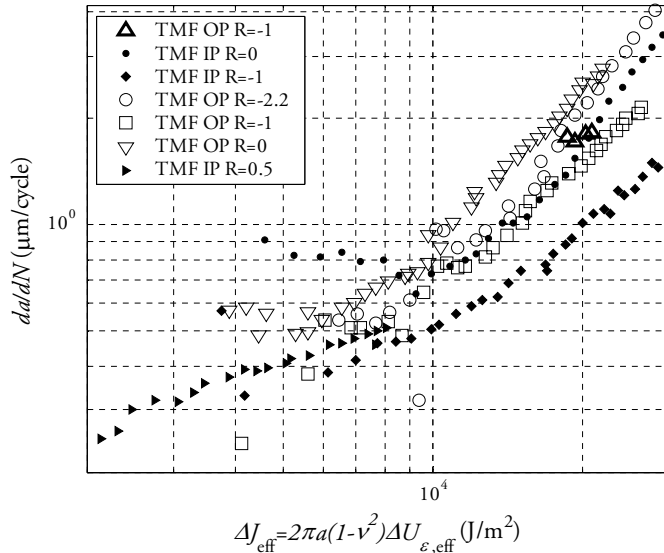


Figure 5. Crack propagation rate versus the effective  $J$ -integral range  $\Delta J_{eff}$ .

### Conclusions

In this work a test facility was developed to be able to perform TMF fatigue crack propagation under controlled forms. Emphasis was put on getting heating and cooling with small thermal gradients over the sample. Heating was obtained by a hot air flow through a nozzle directing the flow towards the sample. Cooling was obtained with a flow of room temperature air through the same nozzle. With the equipment it was possible to obtain TMF cycles with cycle times of 120 s with less than 10°C temperature variation over the measurement length of the sample. The present equipment should be useful for TMF crack propagation tests up to at least 600°C.

The stress intensity factor  $\Delta K$  and the effective  $J$ -integral range  $\Delta J_{eff}$  were used to correlate load to crack propagation range. It was found that the best correlation was obtained with the effective  $J$ -integral range, corrected for crack closure determined using the PD-technique. It was, however, not easy to determine the closure level under TMF cycling conditions, and this is probably the largest source of uncertainty in the results.

Studies of fracture surfaces reveal that the dominant fracture mode was trans-granular crack propagation with striations, indicating a low degree of time dependency. At lower loads, more time dependent failure modes were observed in terms of creep failures of grain boundaries.

### References

- [1] Marchand N, Pelloux R M (1984). Thermal-mechanical fatigue crack growth in Inconel X-750. NASA CR-174835.
- [2] Marchand N, Pelloux R M (1986). A computerized test system for thermal-mechanical fatigue crack growth. *J. of testing and evaluation*, ASTM. 303–311.
- [3] Okazaki M, Yamada H, Nohmi S (1996). Temperature dependence of the intrinsic small fatigue crack growth behavior in Ni-base super alloys based on measurement of crack closure. *Metallurgical and Mat Trans A*, **27A**, 1021–1031.

- [4] Okazaki M, Koizumi T (1987). Relationship of crack growth between thermal-mechanical and isothermal low-cycle fatigue at elevated temperatures. *J. of Eng. Mater. and Techno.*, **109**, 114–118.
- [5] Jordan E H, Meyers G J (1986). Fracture mechanics applied to nonisothermal fatigue crack growth. *Eng. Fract. Mecha.*, **23** (2), 345–358.
- [6] Gemma A E, Langer B S, Leverant G R (1976). Thermo-mechanical fatigue crack propagation in an anisotropic (directionally solidified) nickel-base superalloy. *Thermal Fatigue of Materials and Components*, ASTM STP 612, 199–213.
- [7] Jacobsson L, Persson C, Melin S (2007). In situ scanning electron microscope study of fatigue crack propagation. *Proceedings of 5<sup>th</sup> Int. Conf. on materials structure and micromechanics of fracture*.
- [8] Andersson M, Persson C, Melin S (2006). Experimental and numerical investigation of crack closure mechanisms with electrical potential drop technique. *Int. J. of Fatigue*. **28** (9), 1059–1068.
- [9] Andersson M, Persson C, Melin S (2006). High-temperature fatigue crack growth in Inconel 718 subjected to high strain amplitudes. *Fatigue Fract. Engng. Mater. Struct.* **29**, 863–875.
- [10] Dowling N E, Bagley J A (1976). Fatigue crack growth during gross plasticity and the J-integral. *Mechanics of crack growth*, ASTM STP 560, Society for Testing and Materials, 82–103.
- [11] Lamba H S (1975). The J-integral applied to cyclic loading. *Eng. Fract. Mech.* **7**, 693–703.
- [12] Dowling N E, Iyyer N S (1987). Fatigue crack growth and closure at high cyclic strains. *Mater. Sci. Eng.* **96**, 99–107.
- [13] Meyers J (1982). Fracture mechanics criteria for turbine engine hot section components. NASA report no. 167896.